Phys. Status Solidi B **249**, No. 12, 2436–2441 (2012) / **DOI** 10.1002/pssb.201200152

physica status solidi b
www.pss-b.com
basic solid state physics

# All-optical structure assignment of individual single-walled carbon nanotubes from Rayleigh and Raman scattering measurements

**Stéphane Berciaud*[,1], Vikram V. Deshpande[2,3], Robert Caldwell[3], Yuhei Miyauchi[4], Christophe Voisin[5], Philip Kim[2], James Hone[3], and Tony F. Heinz[2,6]**

[1] Institut de Physique et Chimie des Matériaux de Strasbourg, Université de Strasbourg, CNRS UMR 7504, 23 rue du Loess, BP 43, 67034 Strasbourg Cedex 2, France
[2] Department of Physics, Columbia University, New York 10027, USA
[3] Department of Mechanical Engineering, Columbia University, New York 10027, USA
[4] Institute of Advanced Energy, Kyoto University, Gokasho, Uji, Kyoto 611-0011, Japan
[5] Laboratoire Pierre Aigrain (UMR8551), Ecole Normale Supérieure, CNRS, UPMC and Université Paris Diderot, 75005 Paris, France
[6] Department of Electrical Engineering, Columbia University, New York 10027, USA

Received 8 May 2012, revised 12 September 2012, accepted 19 September 2012
Published online 1 November 2012

**Keywords** carbon nanotubes, excitons, Raman scattering, Rayleigh scattering

* Corresponding author: e-mail stephane.berciaud@ipcms.unistra.fr, Phone: +33-(0)388107256, Fax: +33-(0)388107245

We present an all-optical method for structure assignment of individual single-walled carbon nanotubes (SWNTs) based on combined measurements of the elastically (Rayleigh) and inelastically (Raman) scattered light by individual freestanding specimens. The optical resonances of a single SWNT are identified from the Rayleigh spectra. These measurements are complemented with an independent estimation of the SWNT diameter and chiral angle from its radial breathing and G Raman modes, respectively. An assignment of the $(n,m)$ chiral indices can thus be provided. In the most simple cases, a reliable structure assignment can be inferred from the Rayleigh spectra alone. However, we also show that SWNTs with different structures may display similar Rayleigh spectra within a given photon energy window. In these situations, Raman measurements provide unambiguous criteria for a proper structure assignment. This approach is particularly helpful in order to identify the high-symmetry armchair and zig-zag structures.



**1 Introduction** Single-walled carbon nanotubes (SWNTs) provide a paradigm of quasi one-dimensional nanomaterials with unique physical properties. SWNTs hold great promise for applications in nano-electromechanical devices, nano-electronics, and optoelectronics [1]. SWNTs can be described as rolled-up graphene sheets with diameters in the nanometer range, while their length can exceed one centimeter. The structural parameters (diameter $d$, chiral angle $\theta$) and the electronic structure of a given SWNT can be uniquely described by two integers $(n,m)$ that define the chiral vector in real space connecting two equivalent carbon atoms in the graphene lattice [2, 3]. Consequently a large variety of SWNT species with distinct electronic and optical properties can be formed. The most popular illustration is the existence of 1/3 of metallic species (M-SWNTs, such that $(\nu = [\mathrm{mod}(n-m), 3] = 0)$ and two sub-families of semiconducting species (S-SWNTs, such that $\nu = +1$ and $\nu = -1$) that constitute the remaining 2/3 of SWNT species.

This diversity calls for efficient characterization methods that can operate at the single SWNT level. An all-optical structure assignment scheme, based on combined luminescence and Raman measurements was reported for an ensemble of low diameter S-SWNTs [4]. However this approach is limited to the study of the first two optical resonances ($S_{11}$ and $S_{22}$) and does not apply to M-SWNTs, which do not luminesce. A more direct approach consists in combining a structural and an optical measurements on a same individual SWNT. Combinations of electron diffraction and Raman measurements have made possible the establishment of the relationship between $(n,m)$ and the Raman radial breathing mode (RBM) frequency [5, 6]. Other measurements combining electron diffraction and broad-

band Rayleigh scattering spectroscopy [7] have provided a direct relationship between the optical resonances of a large set of structure-assigned SWNTs, giving access to an empirical Kataura plot for individual M- and S-SWNTs [8]. In this paper, we will describe an all-optical structure assignment scheme that combines inelastic (Raman) and elastic (Rayleigh) light scattering spectroscopy from individual freestanding SWNTs. These measurements can be performed on a simple table-top optical setup and provide a rapid structure assignment, as well as quantitative insights on their optical properties. In particular, we will show that individual M- and S-SWNTs having similar Rayleigh scattering spectra display completely different vibrational properties and electron–phonon coupling, thus providing unambiguous guidelines to distinguish semiconducting and metallic species.

## 2 Trigonal warping (TW) and family behavior

Figure 1 illustrates the basics of the zone folding approximation. In this description, quantum confinement and the boundary conditions (*i.e.*, the diameter and chiral angle of the SWNT) impose a quantization of the transverse momentum according to $k_t = 2/d$, where $d = a\sqrt{n^2 + m^2 + nm}$ and $a = 0.249$ nm denote the diameter and the lattice constant [2, 3]. The electronic subbands of a given $(n, m)$ SWNT are then generated by one dimensional cuts in the two-dimensional dispersion of graphene. These cutting lines are parallel to one another, equally spaced by a distance of $\delta k_t = 2/d$ in the momentum space, and make an angle $\pi/6 - \theta$ with respect to the high symmetry KK′ lines in the Brillouin zone, where $\theta = \arccos\frac{2n+m}{2\sqrt{n^2+m^2+nm}}$ is the chiral angle (see Fig. 1).

A major consequence of the folding is that all SWNTs belonging to the $\nu = 0$ family possess a pair of "Graphene Like subBands" (GLB) crossing the K (or "Dirac") point (*i.e.*, the edge of the graphene Brillouin zone), and are therefore metallic. These SWNTs will exhibit quasi-linear low-energy electronic dispersion, like the "massless dispersion" of graphene. The remaining species from the $\nu = \pm 1$ families have no subband crossing the Dirac point. These SWNTs exhibit a bandgap and are semiconducting. Except for the GLB, the other subbands consist of a set of nearly parabolic bands. Interband absorption across conduction and valence subbands of the same index $i$ is dominated by particularly strong excitonic transitions [9–11], labeled $M_{ii}$ and $S_{ii}$ for M- and S-SWNTs, respectively. Noteworthy, excitonic effects persist in M-SWNTs, with lower exciton binding energies owing to screening by the low energy excitations across the GLB [12–15]. Although it neglects excitonic effects, the zone folding scheme of Fig. 1 is particularly helpful in evaluating the scaling relations and family behaviors that affect the optical resonances. Its most

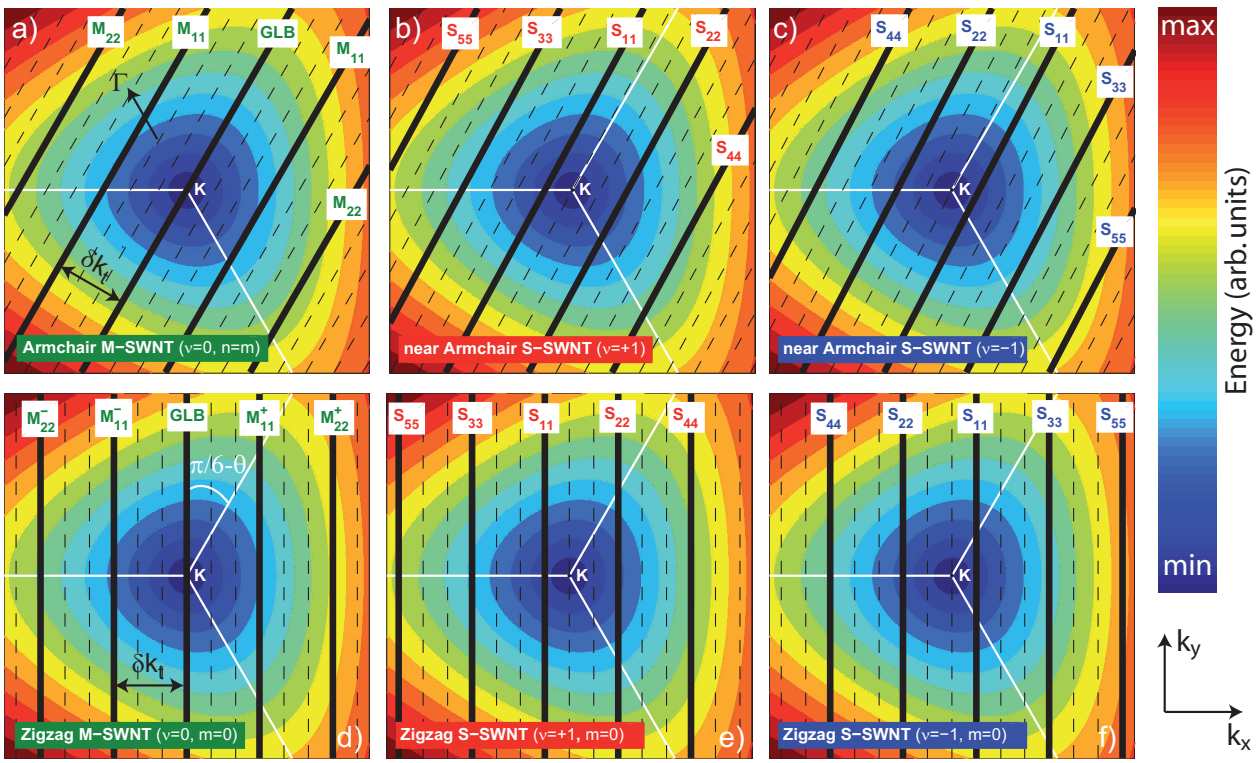


**Figure 1** (online color at: www.pss-b.com) Schematic representation of the zone folding method. The contour plot represents the electronic dispersion of graphene. The cutting lines that define the electronic subbands of a given SWNT are represented by the thick black lines and are equally spaced by a distance taken as $\delta k_t = 0.06\pi/a$ in this illustration. This corresponds to an SWNT diameter of $d \approx 2.6$ nm. Panel (a) corresponds to an armchair M-SWNT ($\theta = \pi/6$). Panels (b) and (c) correspond to a near-armchair S-SWNT from the $\nu = +1$ and $\nu = -1$ family, respectively. Panels (d–f) represent zigzag structures ($\theta = 0$) belonging to the $\nu = 0$, $\nu = +1$, $\nu = -1$ families, respectively.

straightforward consequence is that for a given SWNT diameter (as represented in Fig. 1), M- and S-SWNT will have very different transition energies. As shown in Fig. 1, the first excitonic transition in M-SWNTs ($M_{11}$) will be at significantly higher energy than the $S_{11}$ transition. Provided one can get an independent measurement of the diameter of a given SWNT, for example through its RBM frequency, it will be easy to distinguish an M-SWNT from an S-SWNT from the measurement of its optical resonances.

Another important family behavior arises from TW [16], *i.e.*, the deviation from linearity of the electronic dispersion of graphene as momentum grows away from the K point. This deviation gives rise to the anisotropic contours observed in Fig. 1. Consequently, for non-armchair M-SWNTs (such that $\theta \neq \pi/6$, *i.e.*, the cutting lines are not parallel to the KK′ direction), a pair of cutting lines that is symmetric with respect to K will probe different energy contours. This induces the popular TW splitting in M-SWNTs [17]. As illustrated in Fig. 1, for a given diameter, the TW splitting increases as the chiral angle $\theta$ approaches 0 (*i.e.*, the zigzag structure) and also as the order of the optical transition increases. TW splittings of up to $\sim$400 meV have been observed in zigzag and near zigzag SWNTs [17, 8]. A conceptually similar consequence is that consecutive transitions $S_{ii}$, $S_{i+1,i+1}$ in a given S-SWNTs will have different energy ratio depending on whether the S-SWNT belongs to the $\nu = +1$ or $\nu = -1$ family. In particular, for a given SWNT diameter, as $\theta$ decreases, the $S_{44}/S_{33}$ ratio will increase (decrease) for the $\nu = +1$ ($\nu = -1$) family.

**3 Structure dependent electron–phonon coupling** Owing to the well-defined excitonic resonances, resonant Raman spectra can be recorded for laser photon energies that satisfy an incoming or outgoing Raman resonance. The Raman spectrum of an SWNT is dominated by the radial breathing mode and the zone-center longitudinal (LO) and transverse (TO) optical phonons that compose the G-mode [18]. The frequency of the RBM scales inversely with nanotube diameter. The method of choice to verify this scaling law is to combine electron diffraction and Raman measurements on individual freestanding SWNTs. Two different expressions have been reported, namely, $\omega_{\mathrm{RBM}}(\mathrm{cm}^{-1}) = 27 + 204/d(\mathrm{nm})$ [5] and $\omega_{\mathrm{RBM}}(\mathrm{cm}^{-1}) = 228/d(\mathrm{nm})$ [6]. These two expressions give rise to significant differences for structure assignment, especially in the large diameter limit. However, the choice of expression has no consequence on the family behaviors discussed thereafter.

The zone-center LO and TO modes have equal frequencies in graphene. In SWNTs, however, curvature lifts the degeneracy. This gives rise to bimodal G-modes composed a $G^+$ and a $G^-$ subfeatures [19]. Importantly, coupling to the LO (TO) phonons is absent in armchair (zigzag) SWNTs. In these two limiting cases, the G-mode has a pure TO (LO) character and a single peak is observed [20, 21]. In S-SWNTs, the $G^+$ ($G^-$) feature has a dominant contribution from the LO (TO) phonon. These two peaks have narrow ($\sim$5 $\mathrm{cm}^{-1}$) Lorentzian lineshapes. In M-SWNTs, coupling between zone center LO phonons and low-energy quasiparticles across the GLB gives rise to a significant phonon softening and broadening. This coupling does not affect zone center TO phonon and increases as the chiral angle evolves from an armchair to a zigzag structure [17, 21]. Only in the case of an armchair SWNT is the G mode expected to appear as a narrow TO feature. Otherwise, the G mode spectrum of chiral M-SWNTs is dominated by a broad $G^-$ that arises from the LO phonon, while the $G^+$ feature appears as a narrow Lorentzian peak. In large enough diameter M-SWNTs, the $G^+$ may be appear within the broad $G^-$ feature [13, 17].

## 4 Experimental methods

**4.1 Optical setup and samples** Visible Rayleigh spectroscopy is a powerful technique for studying optical transitions in SWNTs [7, 13, 14, 17, 22, 23]. Recent advances in supercontinuum generation have led to a significantly improved signal-to-noise ratio. Thus, we are able to conduct a reliable lineshape analysis and gain valuable information on the underlying microscopic mechanisms [13]. In our work, we studied the optical response of SWNTs with diameters in the range 1.5–2.8 nm. The samples consist of isolated suspended SWNTs grown by chemical vapor deposition on a silicon substrate over a 100 μm open slit in air [22]. The typical separation between two nearly parallel SWNTs across the slit was much greater than 10 μm. Optical measurements were performed using a home built confocal microscope consisting of a pair of long working distance objective lenses with orthogonal optical axis (see Fig. 2). This arrangement ensures a dark field detection of the Rayleigh (see Fig. 2a) and Raman (see Fig. 2b) scattered light by a single isolated SWNTs with a minimal background. All spectra were recorded by means of a spectrometer equipped with a liquid nitrogen cooled CCD array. Our setup is by no means limited to investigations on large diameter SWNTs bridging wide slits. Measurements on smaller diameter SWNTs grown across narrower apertures (<20 μm) are also possible and will be described elsewhere.

**4.2 Rayleigh and Raman measurements** Rayleigh spectra were obtained over a photon energy range 1.2–2.7 eV. In this range, we are sensitive to the $M_{22}$, $S_{33}$, and $S_{44}$ transitions. For small diameter nanotubes, the $M_{11}$ transition may be observed, while the $S_{55}$ transition may appear below 2.7 eV for S-SWNTs with $d > 2.5$ nm [13]. The raw spectra were corrected for the supercontinuum spectrum and for the $\omega^3$ systematic dependence of the scattering cross-section expected for an infinite cylinder (for details, see Ref. [1, 7]). In contrast to absorption, which only probes the imaginary part of the SWNT dielectric susceptibility $\chi$ [12, 24], the Rayleigh scattering cross section is proportional to $\omega^3|\chi(\omega)|^2$, *i.e.*, it includes response of both parts of $\chi$. Non-resonant contributions to $\chi$, *e.g.*, from the tails of neighboring resonances, or the onset of free-carrier transitions are responsible for the typical asymmetric

 

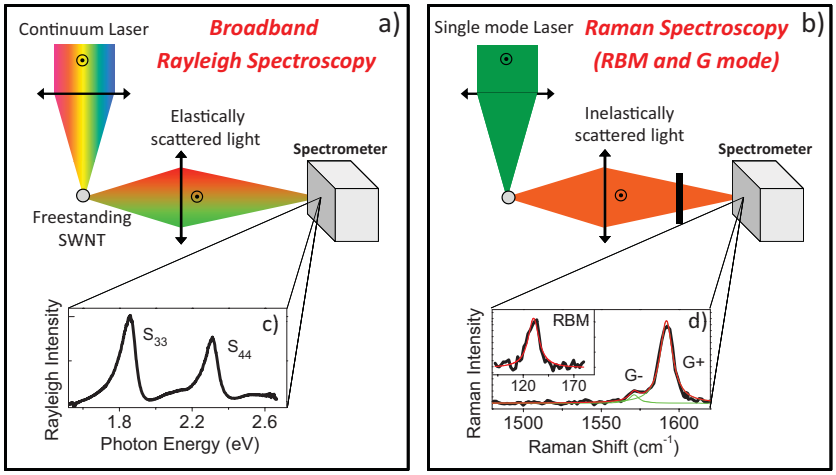


**Figure 2** (online color at: www.pss-b.com) Micro-optical setup for (a) Rayleigh and (b) Raman scattering measurements on individual SWNTs. Typical Rayleigh (c) and Raman (d) spectra are shown for an S-SWNT (NTA) that has been assigned to (16,12) ($d = 1.91$ nm, $\theta = 25.3°$). The red and green lines in (d) are Lorentzian fits of the Raman RBM and G mode features.

lineshapes of the Rayleigh scattering spectra. In order to extract the energies of the optical resonances, we have fit the experimental Rayleigh data to an excitonic model, where the complex susceptibility of the exciton is described by a Lorentzian profile $\chi(\omega) \sim [(\omega_0 - \omega) - i\gamma/2]^{-1}$ where $\omega_0$ is the resonance frequency and $\gamma$ a phenomenological width.

Narrow laser lines at 1.96 and 2.33 eV were used to record micro-Raman spectra. Raman lines were fit to Lorentzian forms or to Breit Wigner Fano profiles in the case of the $G^-$ feature of chiral M-SWNTs [14, 17]. The polarization of the incoming beam was always set parallel to the tube axis and moderate intensities ($\sim$100 kW cm$^{-2}$) were used for all measurements.

**4.3 Structure assignment** A hybrid experimental/theoretical scheme was developed for the assignment of nanotube structure. First, for some key nanotubes the Rayleigh spectra and electron diffraction patterns were both measured [7, 8], with the latter providing direct determination of the ($n$,$m$) chiral indices. Then, for other SWNT structures, the assignments were made not based on the predicted transition energies [25], but rather on the family patterns [4, 7, 8] with the energies adjusted to match the established experimental reference points. The tentative assignments were further confirmed by Raman scattering spectra of the RBM and G modes.

## 5 Results and discussion

**5.1 A simple case: Close-to-armchair S-SWNTs** The Rayleigh and Raman spectra of an individual SWNT (labeled NTA) are shown as a first example in Fig. 2c and d, respectively. The observation of two well defined optical resonances (separated by 450 meV) together with a narrow and bimodal G mode demonstrate that this SWNT is a chiral S-SWNT (cf. Sections and 3). Note that the two prominent exciton-phonon sidebands at $\sim$200 meV are also detected above each optical resonances [13]. Finally, the RBM frequency of 130 cm$^{-1}$ suggests a diameter between 1.75 nm [8] and 2.0 nm [5]. In agreement with the electron diffraction/Rayleigh measurements of Sfeir et al. [7] and Liu et al. [8], this SWNT is assigned to a (16,12) S-SWNT ($d = 1.91$ nm, $\theta = 25.3°$). More generally, the typical $S_{44}/S_{33}$ ratio for $\nu = +1$ S-SWNTs such that $n - m = 1$ is on the order of 1.20. S-SWNTs belonging to the other $\nu = +1$ ($\nu = -1$) sub-families will exhibit an $S_{44}/S_{33}$ ratio greater (lower) than 1.20. The SWNTs shown hereafter in Figs. 3, 4, 5, and 6 are labeled NTB, NTC, NTD, and NTE, respectively.

**5.2 Armchair M-SWNTs versus $\nu = +1$ zigzag S-SWNTs** Figures 3 and 4 display fairly similar Rayleigh spectra with sharp resonances at 1.98 and 1.96 eV, respectively. However, their Raman spectra differ drastically.

First, NTB has a much lower RBM frequency (106 cm$^{-1}$) than NTC (141 cm$^{-1}$). This alone suggests that NTB is metallic, while NTC is semiconducting. This assumption is confirmed by the study of the Raman G-mode. NTB and NTC display narrow Lorentzian G-mode features. Following the discussion in Section 3, this means that these SWNTs are either armchair M-SWNTs or near-zigzag S-SWNTs. We note that the G-mode frequency of NTB (1585 cm$^{-1}$) is significantly lower than that of SWNT NTC (1591 cm$^{-1}$). This strongly indicates that the G-mode of NTB (NTC) is dominated by the TO (LO) zone-center phonon. We conclude that (i) NTB is an armchair M-SWNT of $\sim$2.5–2.7 nm diameter, with an $M_{22}$ transition at 1.98 eV, assigned to (19,19) ($d = 2.58$ nm, $\theta = 30°$) or (20,20) ($d = 2.71$ nm, $\theta = 30°$), and (ii) NTC is a zigzag or near-zigzag tube from the $\nu = +1$ family, with an $S_{33}$ transition at 1.96 eV, assigned to (22,0) ($d = 1.72$ nm, $\theta = 0$) or (21,2) ($d = 1.73$ nm, $\theta = 4.5°$). The absence of an $S_{44}$ up to a photon energy of 2.7 eV, together with the presence of a rising front above $\sim$2.65 eV provides an estimate of $\sim$1.4 for the $S_{33}/S_{44}$ ratio in $\nu = +1$ zigzag S-SWNTs with $d \sim 1.7$ nm.

**5.3 Chiral M-SWNTs versus $\nu = -1$ zigzag S-SWNTs** NTD and NTE, shown in Figs. 5 and 6, respectively, also show fairly similar Rayleigh spectra, yet very different Raman spectra.

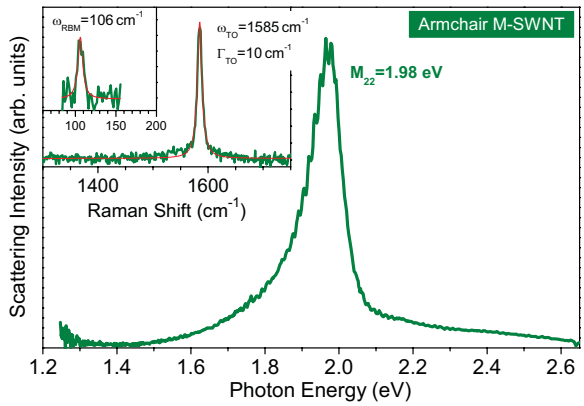


**Figure 3** (online color at: www.pss-b.com) NTB: Rayleigh and Raman spectra of an armchair M-SWNT assigned to (19,19) ($d = 2.58$ nm, $\theta = 30°$) or (20,20) ($d = 2.71$ nm, $\theta = 30°$). The Raman peaks are fit to Lorentzians. The central frequency $\omega$ and full width at half maximum $\Gamma$ are indicated.

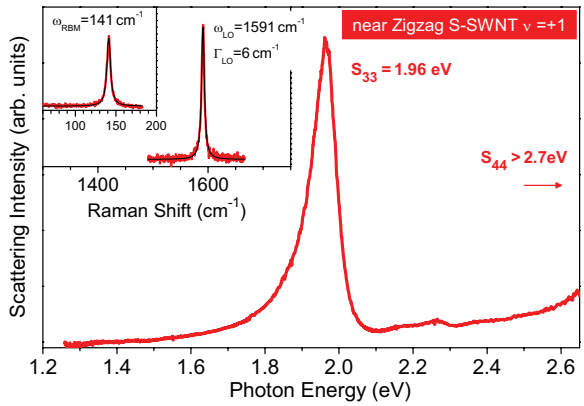


**Figure 4** (online color at: www.pss-b.com) NTC: Rayleigh and Raman spectra of a near zigzag semiconducting SWNT belonging the $\nu = -1$ family, assigned to (22,0) ($d = 1.72$ nm, $\theta = 0$) or (21,2) ($d = 1.73$ nm, $\theta = 4.5°$). The Raman peaks are fit to Lorentzians. The central frequency $\omega$ and full width at half maximum $\Gamma$ are indicated.

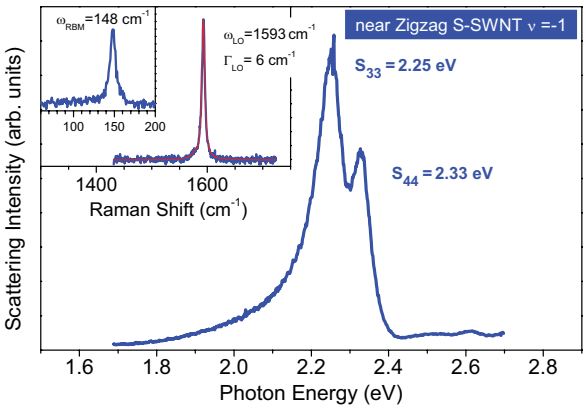


**Figure 5** (online color at: www.pss-b.com) NTD Rayleigh and Raman spectra of a near zigzag semiconducting SWNT belonging to the $\nu = -1$ family, assigned to (20,3) ($d = 1.70$ nm, $\theta = 6.9°$) or (21,1) ($d = 1.69$ nm, $\theta = 2.3°$). The Raman peaks are fit to Lorentzians. The central frequency $\omega$ and full width at half maximum $\Gamma$ are indicated.

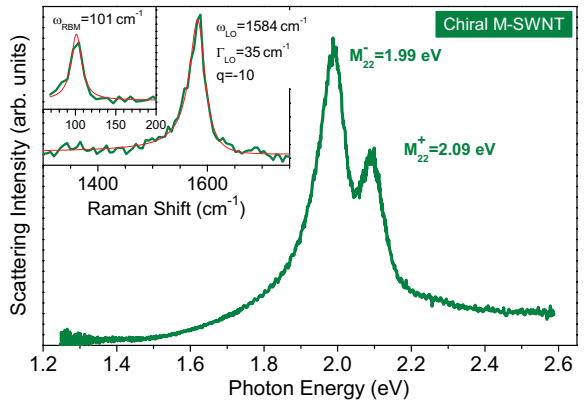


**Figure 6** (online color at: www.pss-b.com) NTE: Rayleigh and Raman spectra of a chiral metallic SWNT assigned to (24,15) ($d = 2.67$ nm, $\theta = 22.4°$). The Raman peaks are fit to Lorentzians. The central frequency $\omega$ and full width at half maximum $\Gamma$ are indicated.

Both Rayleigh spectra are composed of two peaks (at 2.25 and 2.33 eV; 1.99 and 2.09 eV, respectively) separated by less that 100 meV. However, NTD and NTE have RBM frequencies of 148 and 101 cm$^{-1}$, which suggest diameters of $\sim$1.7 nm and 2.7 nm, respectively. In addition, NTD exhibits a single and narrow G-mode feature at 1593 cm$^{-1}$, that indicates a dominant contribution from the LO zone center phonon. NTE displays a much broader, down-shifted and mildly asymmetric G-mode feature (see Fig. 6) that is typical from a chiral M-SWNT [13, 14, 17]. Consequently, the two visible optical resonances of NTD (NTE) are attributed to the $S_{33}$ and $S_{44}$ transitions of a near zigzag S-SWNT belonging to the $\nu = -1$ family (to the $M_{22}^{-}$ and $M_{22}^{+}$ transitions of a chiral M-SWNT). NTD is therefore assigned to a (20,3) ($d = 1.70$ nm, $\theta = 6.9°$) or (21,1) ($d = 1.69$ nm, $\theta = 2.3°$) near-zigzag S-SWNT. The $S_{44}/S_{33} = 1.035$ ratio of NTD provides an estimate for the lowest value obtained in S-SWNTs with $d \sim 1.7$ nm. Combining with the spectral features observed on NTC we conclude that $1.03 < S_{44}/S_{33} < 1.4$ for $d \sim 1.7$. Finally, based on its diameter and the TW splitting of 100 meV, NTE is assigned to a (24,15) M-SWNT ($d = 2.67$ nm, $\theta = 22.4°$).

**6 Conclusions** We have shown that a combinaison of Rayleigh and Raman measurements provides a reliable all-optical structure assignment at the single carbon nanotube level. While structure assignment is rather straightforward in the case of close-to-armchair semiconducting species, we have demonstrated that appearances can be deceptive, and that in many cases, a reliable assignment cannot be made based solely on the analysis of a Rayleigh spectrum. However, complementary Raman measurements of the

radial breathing and G-modes provide decisive information for a structure assignment. For large diameter nanotubes, there exist a few of structures with nearly identical diameter and chiral angle. In these cases, a couple tentative ($n$,$m$) assignments have been proposed. This all-optical assignment scheme will be of great interest for the study of lower diameter nanotubes, for which carrier–carrier interactions, TW and electron–phonon coupling have enhanced effects. Finally, we would like to stress that the recent observation of electronic Raman scattering exclusively in metallic carbon nanotubes provides an additional criterion to distinguish metallic species from semiconducting ones [14].

**Acknowledgements** We acknowledge support from the Nanoscale Science and Engineering Initiative of the NSF under grant CHE-0117752, from the Nanoelectronics Research Initiative of the Semiconductor Research Corporation (NRI-SRC), from the U.S. Department of Energy, Basic Energy Sciences under grant DE-FG02-07ER15842, and from the W. M. Keck Foundation.

## References

[1] A. Jorio, G. Dresselhaus, and M. S. Dresselhaus, Carbon Nanotubes: Advanced Topics in the Synthesis, Structure, Properties and Applications (Springer-Verlag, Berlin, 2009).
[2] R. Saito, G. Dresselhaus, and M. S. Dresselhaus, Physical Properties of Carbon Nanotubes (Imperial College Press, London, 1998).
[3] S. Reich, C. Thomsen, and J. Maultzsch, Carbon Nanotubes: Basic Concepts and Physical Properties (Wiley-VCH, Berlin, 2004).
[4] S. M. Bachilo, M. S. Strano, C. Kittrell, R. H. Hauge, R. E. Smalley, and R. B. Weisman, Science **298**(5602), 2361–2366 (2002).
[5] J. C. Meyer, M. Paillet, T. Michel, A. Moréac, A. Neumann, G. S. Duesberg, S. Roth, and J. L. Sauvajol, Phys. Rev. Lett. **95**(21), 217401 (2005).
[6] K. Liu, W. Wang, M. Wu, F. Xiao, X. Hong, S. Aloni, X. Bai, E. Wang, and F. Wang, Phys. Rev. B **83**, 113404 (2011).
[7] M. Y. Sfeir, T. Beetz, F. Wang, L. M. Huang, X. M. H. Huang, M. Y. Huang, J. Hone, S. O'Brien, J. A. Misewich, T. F. Heinz, L. J. Wu, Y. M. Zhu, and L. E. Brus, Science **312**(5773), 554–556 (2006).
[8] K. Liu, J. Deslippe, X. Fajun, R. B. Capaz, X. Hong, S. Aloni, A. Zettl, W. Wang, X. Bai, S. G. Louie, E. Wang, and F. Wang, Nature Nanotechnol. **7**, 325 (2012).
[9] F. Wang, G. Dukovic, L. E. Brus, and T. F. Heinz, Science **308**(5723), 838–841 (2005).
[10] J. Maultzsch, R. Pomraenke, S. Reich, E. Chang, D. Prezzi, A. Ruini, E. Molinari, M. S. Strano, C. Thomsen, and C. Lienau, Phys. Rev. B **72**(24), 241402 (2005).
[11] C. Voisin, S. Berger, S. Berciaud, H. Yan, J. S. Lauret, G. Cassabois, P. Roussignol, J. Hone, and T. F. Heinz, Phys. Status Solidi B **249**(5), 900–906 (2012).
[12] F. Wang, D. J. Cho, B. Kessler, J. Deslippe, P. J. Schuck, S. G. Louie, A. Zettl, T. F. Heinz, and Y. R. Shen, Phys. Rev. Lett. **99**, 227401 (2007).
[13] S. Berciaud, C. Voisin, H. Yan, B. Chandra, R. Caldwell, Y. Shan, L. E. Brus, J. Hone, and T. F. Heinz, Phys. Rev. B **81**(4), 041414(R) (2010).
[14] H. Farhat, S. Berciaud, M. Kalbac, R. Saito, T. F. Heinz, M. S. Dresselhaus, and J. Kong, Phys. Rev. Lett. **107**, 157401 (2011).
[15] P. May, H. Telg, G. Zhong, J. Robertson, C. Thomsen, and J. Maultzsch, Phys. Rev. B **82**, 195412 (2010).
[16] R. Saito, G. Dresselhaus, and M. S. Dresselhaus, Phys. Rev. B **61**(4), 2981–2990 (2000).
[17] Y. Wu, J. Maultzsch, E. Knoesel, B. Chandra, M. Y. Huang, M. Y. Sfeir, L. E. Brus, J. Hone, and T. F. Heinz, Phys. Rev. Lett. **99**(2), 027402 (2007).
[18] M. S. Dresselhaus, G. Dresselhaus, R. Saito, and A. Jorio, Phys. Rep. **409**, 47–99 (2005).
[19] M. Paillet, T. Michel, J. C. Meyer, V. N. Popov, L. Henrard, S. Roth, and J. L. Sauvajol, Phys. Rev. Lett. **96**, 257401 (2006).
[20] M. Damnjanović, I. Milošević, T. Vuković, and R. Sredanović, Phys. Rev. B **60**, 2728–2739 (1999).
[21] S. Piscanec, M. Lazzeri, J. Robertson, A. C. Ferrari, and F. Mauri, Phys. Rev. B **75**(3), 035427 (2007).
[22] M. Y. Sfeir, F. Wang, L. M. Huang, C. C. Chuang, J. Hone, S. P. O'Brien, T. F. Heinz, and L. E. Brus, Science **306**(5701), 1540–1543 (2004).
[23] D. Joh, L. Herman, S. Ju, J. Kinder, M. Segal, J. Johnson, G. Chan, and J. Park, Nano Lett. **11**(1), 1–7 (2011).
[24] S. Berciaud, L. Cognet, P. Poulin, R. B. Weisman, and B. Lounis, Nano Lett. **7**, (5), 1203–1207 (2007).
[25] V. N. Popov, New J. Phys. **6**, 17 (2004).